Fottea, Olomouc, 22(1): 122–136, 2022
DOI: 10.5507/fot.2021.019

Rhodomonas storeatuloformis sp. nov. (Cryptophyceae, Pyrenomonadaceae), a new cryptomonad from the Black Sea: morphology versus molecular phylogeny

Antonina N. Khanaychenko[1], Olga V. Popova[2], Olga A. Rylkova[1], Vladimir V. Aleoshin[2,3], Larisa O. Aganesova[1] & Maria Saburova[4*]

[1]*A.O. Kovalevsky Institute of Biology of the Southern Seas, Russian Academy of Sciences, Leninskii ave., 38/3, Moscow, 119991, Russian Federation*
[2]*Belozersky Institute for Physico-Chemical Biology, Lomonosov Moscow State University, Leninskye Gory, 1/40, 119991 Moscow, Russian Federation*
[3]*Kharkevich Institute for Information Transmission Problems, Russian Academy of Sciences, Bolshoy Karetny per., 19/1, 127051 Moscow, Russian Federation*
[4]*Environment and Life Sciences Research Center, Kuwait Institute for Scientific Research, P.O. BOX 1638, Salmiya 22017, Kuwait; *Corresponding author e–mail: msaburova@gmail.com*

Abstract: We established a new cryptomonad species, *Rhodomonas storeatuloformis* sp. nov., based on morphological and molecular characters of cultured strain isolated from the Black Sea. Cells are slightly dorsoventrally flattened, obloid in shape, 12–19 µm in length and 5–10 µm in width, with light–brown, parietal H–shaped chloroplast and a central pyrenoid. Two unequal flagella are located subapically in a short V–shaped vestibulum with a ligule on the left side. Cells are covered by a sheet–like papillate perisplast with numerous small underlain ejectosomes; discharged ejectosomes form distinctly visible minute pores. Mid–ventral band is absent. In general, cell morphology is very similar to described strains of *Storeatula* genus. However, phylogenetic analyses based on sequences of the partial nuclear 18S, 28S rDNA, and complete internal transcribed spacer (ITS) region of rDNA placed the novel cryptomonad strain within *Rhodomonas* genus as a separate clade. The predicted secondary structure of nuclear rDNA ITS2 has numerous compensatory base changes compared to the closest relative strains that support the distinction of the novel species among *Rhodomonas* taxa. The present results contribute to the study on still hidden cryptomonad biodiversity in the Black Sea. Contradiction between morphology and phylogenetic data in *R. storeatuloformis* further argues for revision of the generic delineations in the family Pyrenomonadaceae.

Key words: Black Sea, compensatory base changes, ITS2; rDNA phylogeny, *Rhodomonas storeatuloformis* sp. nov., SEM, taxonomy

Introduction

Cryptomonads (=cryptophytes) are ubiquitous small unicellular biflagellate protists that are playing an important role in organic carbon cycle in a wide range of marine, brackish, and fresh water environments worldwide (Klaveness 1988; Buma et al. 1992; Kugrens et al. 1999; Han & Furuya 2000; Novarino 2005; Cerino & Zingone 2006; Hoef–Emden 2008; Medlin & Schmidt 2010; Hoef–Emden & Archibald 2016; Medlin et al. 2017; Altenburger et al. 2020; Gusev et al. 2020). Cryptomonads include autotrophic and mixotrophic species (Gervais 1997; Roberts & Laybourn–Parry 1999; Hammer & Pitchford 2006; Czypionka et al. 2011; Hoef–Emden & Archibald 2016; Yoo et al. 2017) widespread from the Arctic (Krasnova et al. 2014) to Antarctic (Marshall & Laybourn–Parry 2002). These organisms can cause non–toxic red tides (Laza–Martínez 2012 and references therein; Šupraha et al. 2014; Polikarpov et al. 2020), and are effectively consumed by heterotrophic dinoflagellates (Fields & Rhodes 1991; Adolf et al. 2007), ciliates (Roberts & Laybourn–Parry 1999; Johnson et al. 2016) and copepods (Nakamura & Hirata 2006; Zhang et al. 2013; Khanaychenko et al. 2018). Various cryptomonad strains studied in experimental trophic chains and in marine aquaculture are proved to be an excellent food for cultivating zooplankton including copepods, rotifers and *Artemia* (Støttrup et al. 1986; Khanaychenko 1999; Seixas et al. 2009; Zhang et al. 2013; Coutinho et al. 2020; Kim et al. 2020) due to their high production of commercially valuable compounds such as amino

acids, polar lipids and unsaturated eicosapentaenoic and docosahexaenoic fatty acids (Bermúdez et al. 2004; Dunstan et al. 2005; Peltomaa et al. 2018).

Marine cryptomonads are still poorly studied in terms of their biodiversity, distribution and food web interactions despite their widespread occurrence in coastal ecosystems. Recent studies have shown the key role of cryptophytes as a food resource for cyclopoid copepods, which, in their turn, are an important food source for fish larvae (Khanaychenko et al. 2018). Cryptomonad abundance in the Black Sea coastal waters varied seasonally between 10^4 and 10^6 cells L^{-1} (unpublished data of the first author), similar to records in other coastal environments worldwide (from 10^4 up to 10^7 cells.l^{-1}; Han & Furuya 2000; Medlin & Schmidt 2010; Šupraha et al. 2014). Despite long–term monitoring of the phytoplankton diversity and ecology in the Black Sea since the late 19th century, taxonomic surveys of cryptomonads deeper than the class level are scarce, mostly based on light microscopy observations of the gross cell morphology, and are often restricted to dominant genera or species. Recent basin–scale assessments of cryptomonad diversity in the Black Sea ranged from 1–2 species commonly occurred in the Russian and Turkish coastal waters to 20 taxa encountered along the Bulgarian coast (Moncheva et al. 2019). M. Rouchijajnen has described several *Cryptomonas* taxa during 1960–70s from the Sevastopol Bay, NW Black Sea (Rouchijajnen 1967, 1970, 1971). Presently, 7 cryptothyte species were reported from the Crimean coastal waters, of which 5 taxa belong to the genus *Cryptomonas* (Senicheva 2008), and 11 cryptomonad taxa were listed in the phytoplankton composition in the Odessa Bay and the adjacent waters (Nesterova et al. 2006). Meanwhile, the proper identification of cryptomonads at the modern level is increasingly important for tracking changes in biodiversity and predicting the ongoing environmental changes. In the Mediterranean Sea, which is the closest basin to the Black Sea, the high diversity of cryptomonads was revealed with at least 16 different morphotypes identified (Cerino & Zingone 2006).

The number of described cryptomonads is about 200 species and probably underestimated (Hoef–Emden et al. 2002), and their precise identification and taxonomy are still unresolved (Hoef–Emden & Archibald 2016). Living cryptomonad cells are easily recognizable under light microscopy (LM) at the class level by their asymmetrical shape and characteristic swimming behavior. However, LM observations are unable to distinguish the external and internal cell ultrastructures, which are important to identify the genera and species of cryptomonads. Moreover, many cryptomonad taxa lack distinctive morphological characters at species level, so the full characterization of new cryptophyte species is based on combination of microscopic techniques (light and electron microscopy) and molecular analyses (Cerino & Zingone 2007; Hoef–Emden 2007; Novarino 2012).

The revealing of the hidden biodiversity of the Black Sea cryptomonads is an ongoing research in the Institute of Biology of the Southern Seas (IBSS) of the Russian Academy of Sciences. This survey is based on a recently established collection of cryptomonad clonal cultures isolated from the Black Sea waters over the years. The present study aims to characterize a strain from this collection on the basis of light and scanning electron microscopic observations and phylogenetic analyses of the ITS region and the 18S and 28S nuclear rDNA genes sequences.

Materials and Methods

Isolation and culture maintenance. The cryptomonad strain IBSS–59 was isolated from the coastal water of the Black Sea in Sevastopol Bay (44°37'00"N, 33°31'18"E) in 2004 by Olga Galatonova (IBSS). Since isolation, the strain was purified and deposited in monospecific culture at Culture Collection of Marine Algae (CCMA) in IBSS. The non–axenic clonal culture of the strain IBSS–59 was routinely maintained at ~44 $mE.m^2.s^{-1}$ light intensity under a 14:10 light:dark photoperiod at 21±2 °C. The culture was diluted in 30% volume every 3–4 days with sterilized seawater (salinity of 18) with half Walne medium to support exponential growth (Andersen 2005).

Light microscopy. Live cells were isolated by micropipetting and transferred to a glass slide for high–magnification photomicroscopy preparation. Cells were observed and measured alive to prevent the shrinkage that may occur after fixation (Novarino 2005) under the inverted microscopes Nikon Eclipse MS 100 and Nikon Eclipse TS2R (Nikon Metrology NV), and under upright microscopes Olympus CX41 (Olympus Corporation, Japan) and Leica DMLM (Leica Microsystems, Germany) equipped with Nomarski differential interference contrast (DIC) optic. Images were taken using digital camera

Table 1. Primers used for PCR and sequencing.

Cell compartment	Gene	Primer	Sequence	Reference
nuclear	18S	18d3	5′–TGGAGGGCAAGTCTGGTG–3′	Milyutina et al. 2001
nuclear	28S	28r3	5′–CCTTGGTCCGTGTTTCAAGAC–3	Van der Auwera et al. 1994
plastid	16S	27F	5′–AGAGTTTGATCMTGGCTCAG–3′	Bourrain et al. 1999
plastid	16S	1525R	5′–AAGGAGGTGWTCCARCC–3′	Bourrain et al. 1999

Fottea, Olomouc, 22(1): 122–136, 2022
DOI: 10.5507/fot.2021.019

Olympus CX41–Infinity at magnification 400× and Leica DFC 320 color digital camera at 1000× magnification. Cell dimensions, presence of different inclusions, position of the pyrenoid and the shape of the plastid were examined from > 100 live cells. Cell length, width and depth were measured from randomly chosen cells, and the range, mean values and standard deviation were calculated.

Scanning electron microscopy. 2 ml of dense strain IBSS–59 were fixed for 60 min in a 1% Lugol's solution (Bistricki & Munawar 1978; Dolgin & Adolf 2019). After fixation, sample was gently concentrated under a vacuum of < 0.2 atm onto a polycarbonate filter (2 µm pore size, Dubna, Russia) in a filter funnel (Sartorius, Germany). After precipitation on a filter, cells were rinsed with distilled water three times, and then were gradually dehydrated through an ethanol series (30%, 50% for 5 min; 75%, 96% for 10 min; 100% twice for 10 min). Filters were dried using automated critical point dryer Leica EM CPD300 (Leica Microsystems, Germany) for 1.5–2.5 h. The dried filters were mounted on alluminium stubs using carbon adhesive tabs and sputter–coated with Au/Pd using vacuum coater Leica EM ACE200 for 1.0 min before visualization with Hitachi SU3500 (Hitachi High Tech, Japan) scanning electron microscope (SEM).

DNA extraction, PCR, and sequencing. DNA was extracted from the strain IBSS–59 using DIAtom DNA Prep kit (Isogen, Russia) following the protocol provided by the manufacturer. We selected common nuclear rDNA and plastid 16S rDNA markers. Partial nuclear encoded 18S (SSU) and 28S (LSU) rDNA and complete internal transcribed spacer (ITS) regions were amplified using primers described earlier (Table 1) with Encyclo PCR kit (Evrogen, Russia).

The PCR cycling conditions included denaturation at 95 °C for 5 min, followed by 40 cycles of denaturation at 95 °C for 30 s, annealing at 55 °C for 30 s, extension at 72 °C for 3 min, and final extension at 72 °C for 5 min. PCR products were separated with agarose gel electrophoresis and purified using Cleanup Mini kit (Evrogen, Russia). Amplicons were sequenced directly with an Applied Biosystems 3730 DNA Analyzer. The sequences of the strain IBSS–59 were deposited in GenBank with accession numbers MW691985 (nuclear rDNA) and MW691986 (plastid 16S rDNA).

Phylogenetic analyses. To place the strain IBSS–59 correctly within Cryptophyceae, at first, we aligned its nucleus–encoded 18S rRNA gene sequences together with a large set of Cryptophyceae sequences (1257 in total) available from GeneBank (from genera *Rhodomonas*, *Pyrenomonas*, *Rhinomonas*, *Storeatula*, *Geminigera*, *Chroomonas*, *Plagioselmis*, *Teleaulax*, *Urgorri*, *Hanusia*, *Guillardia*, *Cryptomonas*, *Chilomonas*, *Falcomonas*, *Proteomonas*, *Hemiselmis*, *Komma*, *Goniomonas*) with katablepharid as an outer sister group. All sequences were aligned in MEGA 6.0 (Tamura et al. 2013) with MUSCLE (Edgar 2004) and manually adjusted in BioEdit (Hall 1999) to a gapped alignment. Phylogenetic inference analysis was performed with IQ–TREE (Nguyen et al. 2015) under the ModelFinder method (–m MFP) and ultrafast bootstrap (–bb 1000). The Symmetric model with unequal rates but equal base frequencies with six FreeRates (SYM+R7) was selected as the best model according to BIC and AIC. The initial phylogenetic tree was visualized with MEGA 6.0 (Tamura et al. 2013). At the initial tree the

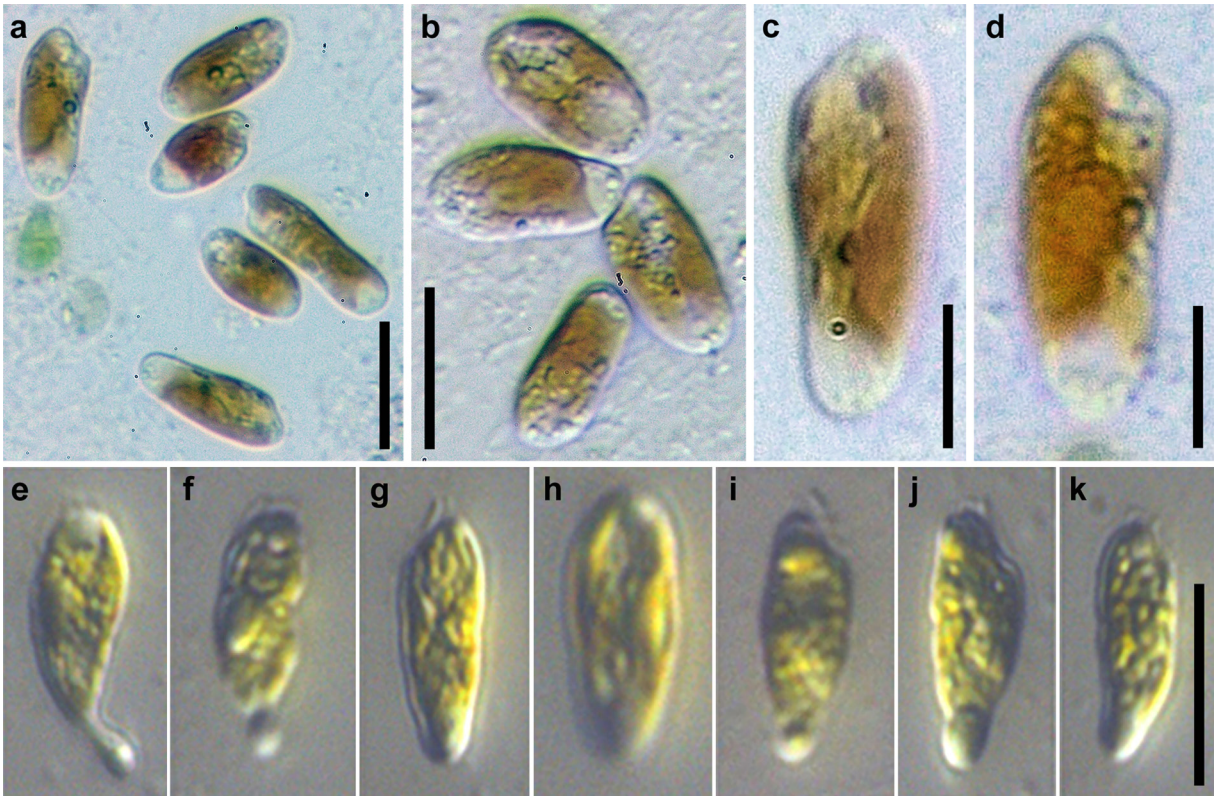

Fig. 1. Light micrographs of *Rhodomonas storeatuloformis* sp. nov. (strain IBSS–59): (a, b) non–motile cells; (c, d) the same cell showing from different sides; (e–k) micrographs of moving cells showing shape variability, Nomarski differential interference contrast. Scale bars 10 µm in (a, b, k) and 5 µm in (c, d), scale bar in (k) valid for (e–j).

strain IBSS–59 groups within family Pyrenomonadaceae with high support (bootstrap value of 100). Secondly, to ensure the placement of the strain IBSS–59 within Pyrenomonadaceae, we removed non–Pyrenomonadaceae sequences as well as redundant sequences with over 98% similarity from the initial alignment. Then we downloaded from GenBank 5.8S, 28S rDNA, and ITS sequences for remaining strains and aligned each type of them separately in MEGA 6.0 with MUSCLE and visual control in BioEdit. Finally, we concatenated the 18S alignment with 5.8S, 28S rDNA, and ITS alignments. The number of sequences in the final alignment was 40 (38 strains of the family Pyrenomonadaceae and *Proteomonas sulcata* and *Falcomonas daucoides* as outgroup). Accession numbers of the final sequences are provided in the phylogenetic tree.

Bayesian inference analysis was performed with MrBayes 3.2.6 (RONQUIST et al. 2012) in two runs under nst=6 ngammacat=8 rates=invgamma parameters, five gene partitions (for 18S, ITS1, 5.8S, ITS2, and 28S sequences), 5000000 generations. For the final ensemble the first 40% of the chains were discarded as burn–in. Average standard deviation of split frequencies was 0.7% after 5000000 generations. Convergence between runs was reached since the PSRF (GELMAN & RUBIN 1992) was 1.0 for all estimated parameters. Maximum likelihood bootstrap support values were calculated from 100 replicates (–b 100), using IQ–TREE under the ModelFinder method (–m MFP). The General Time Reversible with Invariant Sites and four discrete Gamma categories model (GTR+I+G4) was selected as the best model according to BIC and AIC. The phylogenetic tree was visualized with MEGA 6.0 (TAMURA et al. 2013).

Secondary structure prediction. The secondary structures of nucleus–encoded ITS2 sequences of the strain IBSS–59 and four closest strains (*Rhodomonas lens* CCMP739 and *Rhodomonas* spp. CCMP743, CCMP763, and CCMP760) were predicted using the RNA folding program available at the mfold server (http://mfold.rna.albany.edu/?q=mfold/RNAFolding–Form) (ZUKER 2003) with default values. All predicted structures of ITS2 were manually examined and compared for common stems, loops, and bulges. Compensatory base changes (CBCs) in different helices were manually identified from the ITS2 secondary structures of the closest to strain IBSS–59 cryptomonad strains.

RESULTS

***Rhodomonas storeatuloformis* sp. nov. Khanaychenko, Saburova, Aleoshin, Rylkova, Popova et Aganesova (LM, Figs 1, 2; SEM, Fig. 3; Molecular Diagnosis, Figs 4–6)**

Description: Ellipsoid elongated cells are slightly dorsoventrally flattened, obloid in shape; range from 12 to 20 μm in length, and from 5 to 10 μm in width. Parietal H–shaped chloroplast has a central pyrenoid. Cells have two unequal flagella located subapically in a short V–shaped vestibulum with a ligule on the left side. Cells are covered by a sheet–like papillate periplast with numerous small underlaid ejectosomes. Discharged ejectosomes form distinct minute pores. Mid–ventral band and furrow are absent.

Holotype: the SEM stub containing fixed, critical point dried material from the strain IBSS–59, deposited at the Algal Herbarium (LE) of the Komarov Botanical Institute, St. Petersburg, Russia (identification number LEA0000279). A type specimen in ventro–apical view is illustrated in Fig. 3a. Figs 3, c and e–h illustrate other specimens from this stub.

Type locality: Sevastopol Bay (44°37'00"N, 33°31'18"E), the Black Sea.

Habitat: marine coastal waters, plankton.

Etymology: *R. storeatuloformis* is named after similar morphology with *Storeatula* species.

Reference strain: the strain IBSS–59 deposited at Culture Collection of Marine Algae (CCMA) of IBSS.

Gene sequences: DNA sequences are deposited in GenBank under accession numbers MW691985 (nuclear SSU, ITS, and LSU rDNA); MW691986 (plastid 16S rDNA). Nuclear 18S rRNA gene variable region V4: 5′–TCTACTTCATTGTAGGGTTGTGAAACGCAA–3′. Nuclear ITS2 helix II specific motif: 5′–TTCTGAAGGAA–3′. Nuclear ITS2 helix III specific motif: 5′–ACCCTG[N_{81}]AAGTGT–3′. Nuclear ITS2 helix IV specific motif: 5′–GAATTACAGTTC–3′. Species differs from others of the genus by the order of the nucleotides in nuclear ITS, LSU and SSU rDNA gene sequences.

Morphological observations: Culture of *Rhodomonas storeatuloformis* (strain IBSS–59) with cell concentration higher than 10^4 cells.ml^{-1} is characterized by light brown color due to the presence of phycoerythrin in plastids (Fig. S1). High phycoerythrin content in the cells of IBSS–59 strain was confirmed by distinct orange fluorescence with strong emission peak at 575 nm with flow cytometry (KHANAYCHENKO et al. 2018). The motile cells frequently change moving direction and swim forward at relatively low speed rotating around their anterior–posterior axis. Non–motile cells were observed in ageing cultures, forming a layer on the bottom of the vessel and varying considerable in shape and size (Figs 1, a and b). Live motile cells are 12–19 μm in length (14.7 ± 1.7, n=40) and 5–10 μm in width (6.3 ± 1.1, n=40). The cells are ellipsoid elongated in dorsal or ventral view, obloid in shape, with width to length proportions of 2.5 ± 0.5 and a minor dorso–ventral compression. The anterior cell end is rounded in ventral view, and slightly rhinose from lateral view (Figs 1, c and d; 2, c, e, h and k); slightly bended antapex is narrowed toward the end (Figs 1, g–i and k; 3, b and c). Some cells possess the extending "tail–like" hyaline protrusion of antapex (Figs 1, e, f and j; 3d). Two unequally long flagella (Figs 2, a and i–k) are protruding from the V–shaped, widely opened subapical vestibulum (Fig. 3a) with a small ligule on the left side (Fig. 3g). Short gullet is lined with rows of large ejectosomes (Figs 2, e, f, h and l). Ventral flagellum is of approximately the cell length (Fig. 3e) and slightly longer than the dorsal one (Figs 3, e, f and h). Large contractile vacuole is located at the apical (Figs 1, h and i) or anterior (Figs 2, f and g) part of the cell. Nucleus is located in the posterior half of the cell (Figs 1, i and j; 2, a, g, i and j). A single pyrenoid surrounded

Fottea, Olomouc, 22(1): 122–136, 2022
DOI: 10.5507/fot.2021.019

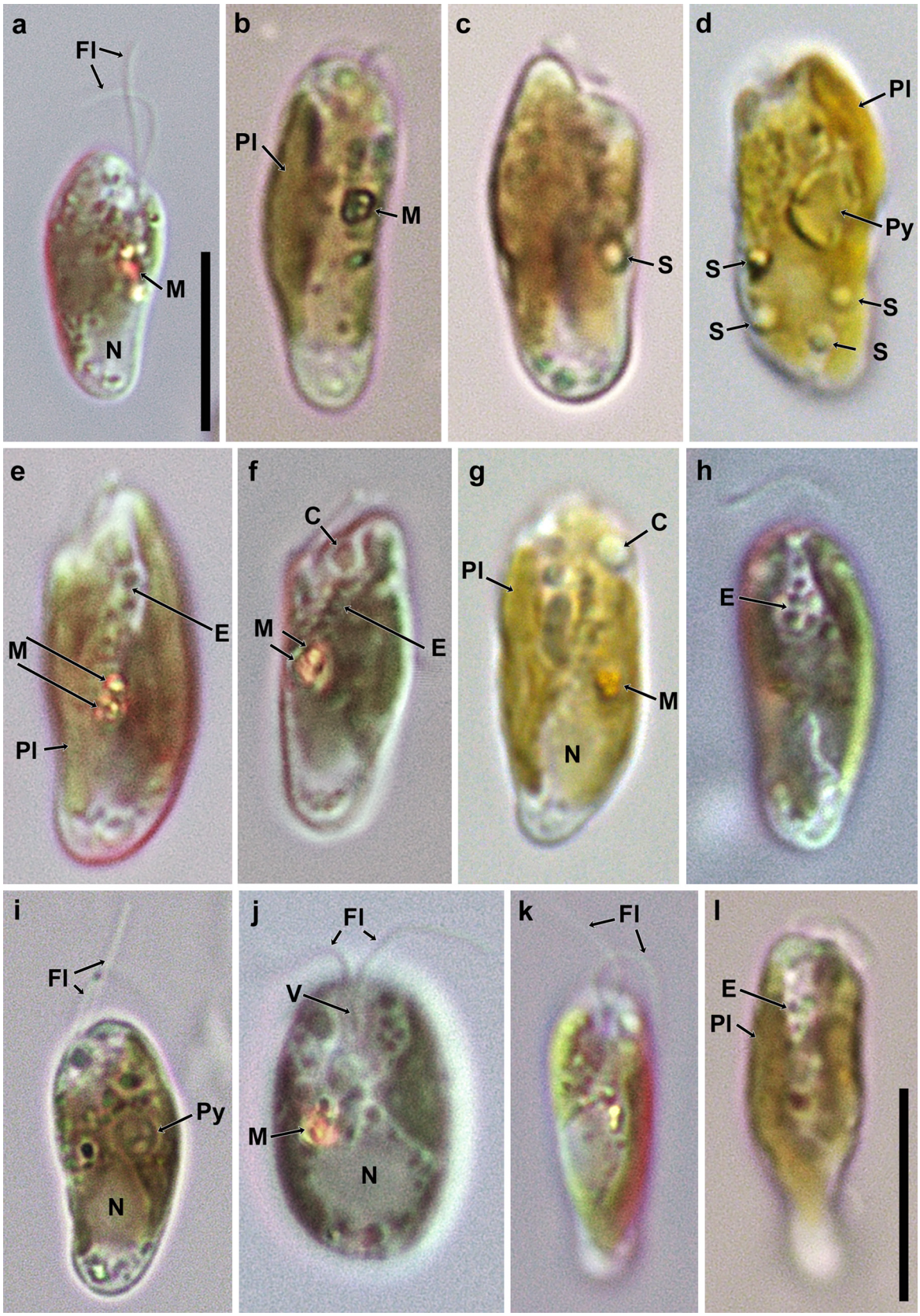

Fig. 2. Light micrographs of *Rhodomonas storeatuloformis* sp. nov. (strain IBSS–59): (a–d) lateral right–sided view; (e, f) lateral left–sided view; (g) ventro–lateral left–sided view focused onto pyrenoid that bridges lobes of chloroplast; (h–l) ventral view. Cells at different focal planes showing two flagella (Fl; a, i–k), single plastid (Pl; b, d, g, l), large single pyrenoid (Py; d, i), refractive and closely spaced maupas ovals (M; a, b, e–g, j), starch grains in posterior part of the cells (S; c, d), anterior contractile vacuole (C; f, g), posterior nucleus (N; a, g, i, j), vestibulum (V; j), and rows of large ejectosomes lined gullet (E; e, h, l). Scale bars 10 μm (a, l), scale bar in (l) valid for (b–k).

by a starch sheet is located in the middle of the cell (Figs 2, d, g and i) between two parts of light brownish parietal bilobed chloroplast (Figs 1, c and d; 2, d, e, g and l). Two highly refractive and closely spaced bodies (maupas ovals) are visible towards the mid of the cell (Figs 2, a, b, e–g and j). Few large starch grains are scattered through the posterior cell part (Figs 2, c and d). The furrow and mid–ventral band are absent. Periplast lacks any plates and consists of the sheet–like layer covering the entire cell surface (Figs 3, a and c). Numerous small underlain ejectosomes bulge the periplast, giving its surface a papillary appearance due to protruding vesicles. Periplast surface is covered by distinctly visible tiny pores formed by discharged underlying ejectosomes (Figs 3, a, c and g). Undischarged ejectosome vesicles are concentrated toward antapex (Fig. 3h).

Molecular phylogeny: Partial nuclear encoded rDNA region and plastid 16S rRNA gene were sequenced from the cultured strain IBSS–59 to clarify the phylogenetic relationship of a novel cryptomonad species *Rhodomonas storeatuloformis*. The sequences were deposited in GenBank with accession numbers MW691985 and MW691986. Phylogenetic analyses based on the partial nuclear SSU and LSU rDNA sequences and complete 5.8S rDNA, ITS1, and ITS2 sequences of 38 cryptomonad strains of the family Pyrenomonadaceae placed *R. storeatuloformis* (strain IBSS–59) among other *Rhodomonas* strains (Fig. 4). *R. storeatuloformis* groups with *Rhodomonas* sp. CCMP743 with bootstrap support of 100 and posterior probability of 1.0. These two strains together with *Rhodomonas* sp. CCMP763 and *Rhodomonas* sp. CCMP762 form a well–supported clade with bootstrap support 100 and 1.0 posterior probability. This clade groups with *Rhodomonas* lineages including *R. lens*, *R. baltica*, and five unidentified *Rhodomonas* strains. Genus *Rhodomonas* is not monophyletic: besides some *Rhinomonas* spp. dispersed among *Rhodomonas* spp.,

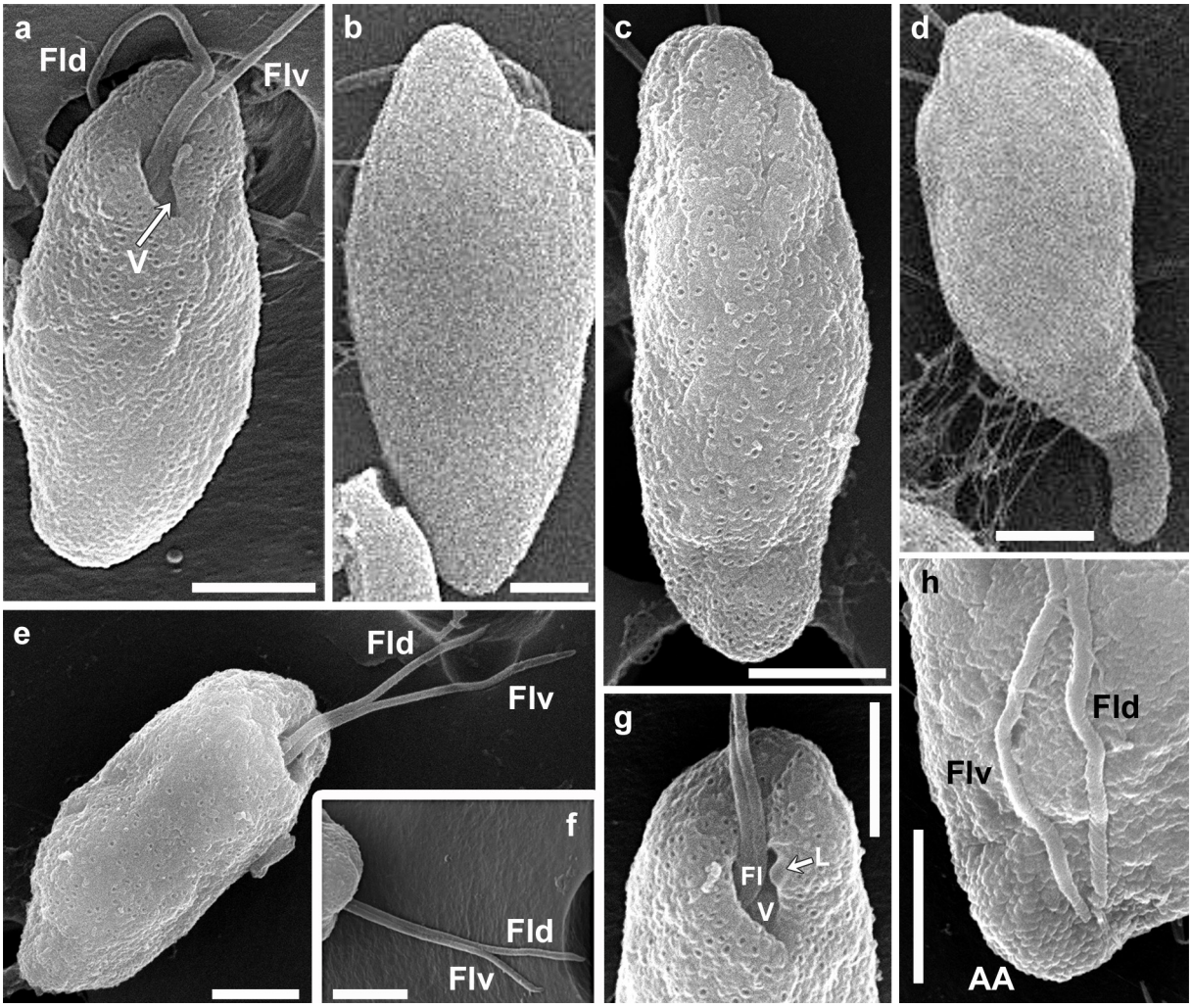

Fig. 3. SEM micrographs of *Rhodomonas storeatuloformis* sp. nov. (strain IBSS–59): (a) ventro–apical view; (b) dorso–lateral view with typical rhinote part of apex and narrow–rounded antapex; (c) dorso–lateral right–sided view; (d) dorso–lateral view of the cell with prominent "tail–like" hyaline antapex; (e, f) lateral right–sided view showing the ventral flagellum being longer than the dorsal one; (g) ventro–apical view showing vestibulum with a small ligule on the left side, note numerous small pores on the periplast produced by the discharge of ejectosomes; (h) ventro–antapical view showing undischarged ejectosome vesicles on antapex and the length of flagella reaching approximately the cell length. (V) vestibulum; (L) ligule; (Fld) dorsal flagellum; (Flv) ventral flagellum; (Fl) flagella; (AA) antapex. Scale bars 2 μm.

Fottea, Olomouc, 22(1): 122–136, 2022
DOI: 10.5507/fot.2021.019

there is a clade within *Rhodomonas* lineages, which includes *Storeatula major* and uncultured cryptophyte Cr–MAL03. Despite *R. storeatuloformis* is most closely related to several *Rhodomonas* strains, it differs from them by the SSU rDNA, LSU rDNA and ITS rDNA sequences. The 5.8S rDNA sequence regions of all strains have the same length, while the lengths of ITS1 and ITS2 differ among strains (Table 2).

Secondary structures of nuclear ITS2 regions: To confirm that *R. storeatuloformis* is a separate species, we compared its nuclear ITS2 structure with homologous ITS2 structures of closely related strains selected according to the phylogenetic tree (Fig. 4) for detection of CBCs. The predicted ITS2 secondary structure of *R. storeatuloformis* folded into a typical structure with four common major helices as in most eukaryotes (Coleman 2007), with the longest helix III, and a typical unpaired U–U in helix II (Fig. 5).

The predicted secondary structures of ITS2 of four closest to *R. storeatuloformis* strains (*R. lens* CCMP739, *Rhodomonas* spp. CCMP743, CCMP763, and CCMP760) were constructed from the GenBank data sequences. Among these strains, all helices are variable in structure

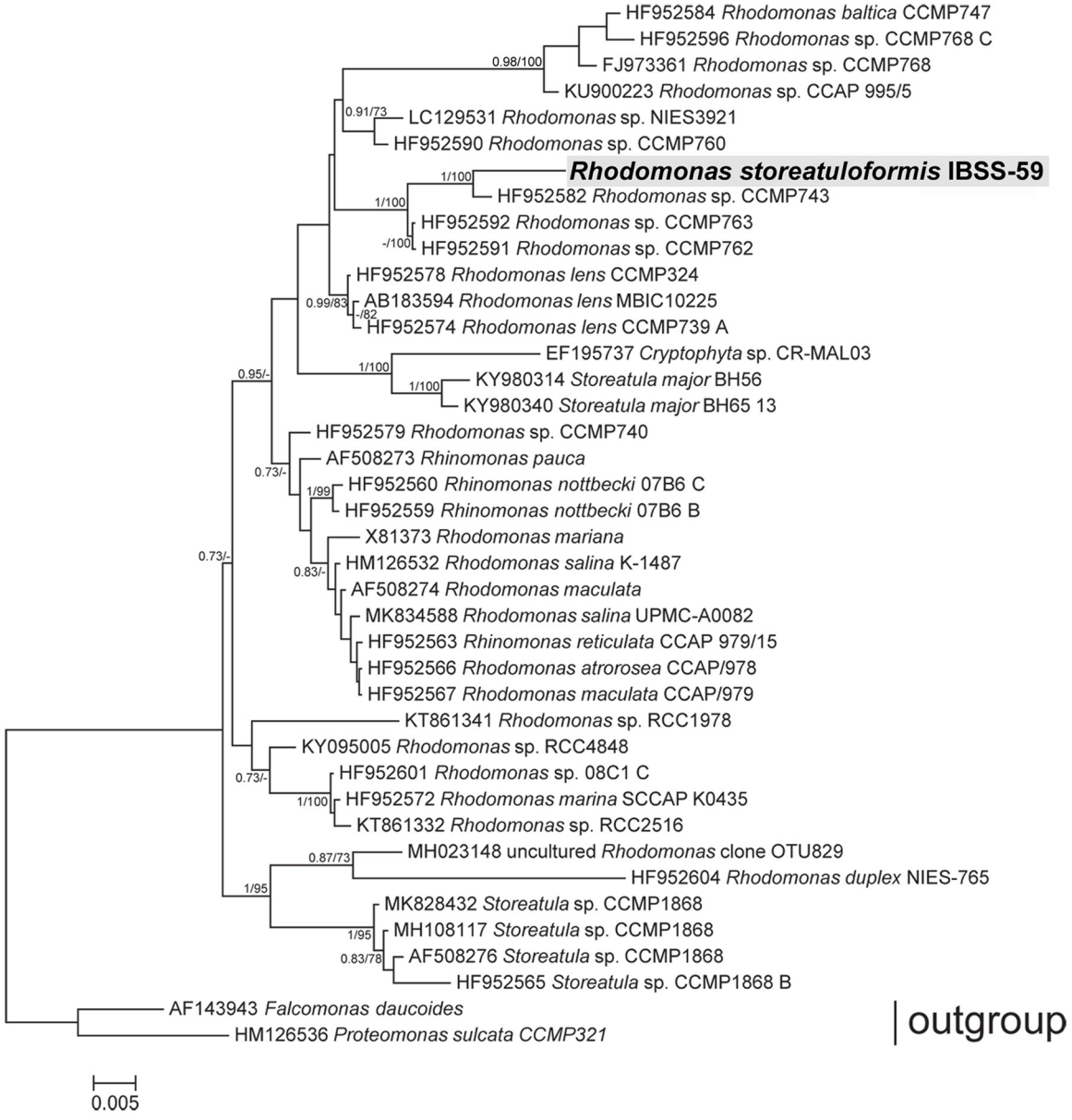

Fig. 4. Bayesian tree based on the concatenated nuclear–encoded 18S rRNA gene, ITS region, and 28S rRNA gene of the family Pyrenomonadaceae members. The sequences are denoted with the strains names, and/or accession numbers (derived from GenBank). Posterior probabilities (left) and maximum likelihood bootstrap support values (right) are shown near the internal nodes. Parameter values which are lower than 0.7 or 70 are labelled with "–". Posterior probabilities were calculated across the GTR+I+G8 model, while the maximum likelihood bootstrap values were calculated with the GTR+I+G4 model. *Rhodomonas storeatuloformis* sp. nov. (strain IBSS–59, accession number MW691985) is highlighted in bold and shaded gray. Scale bar: substitution per site.

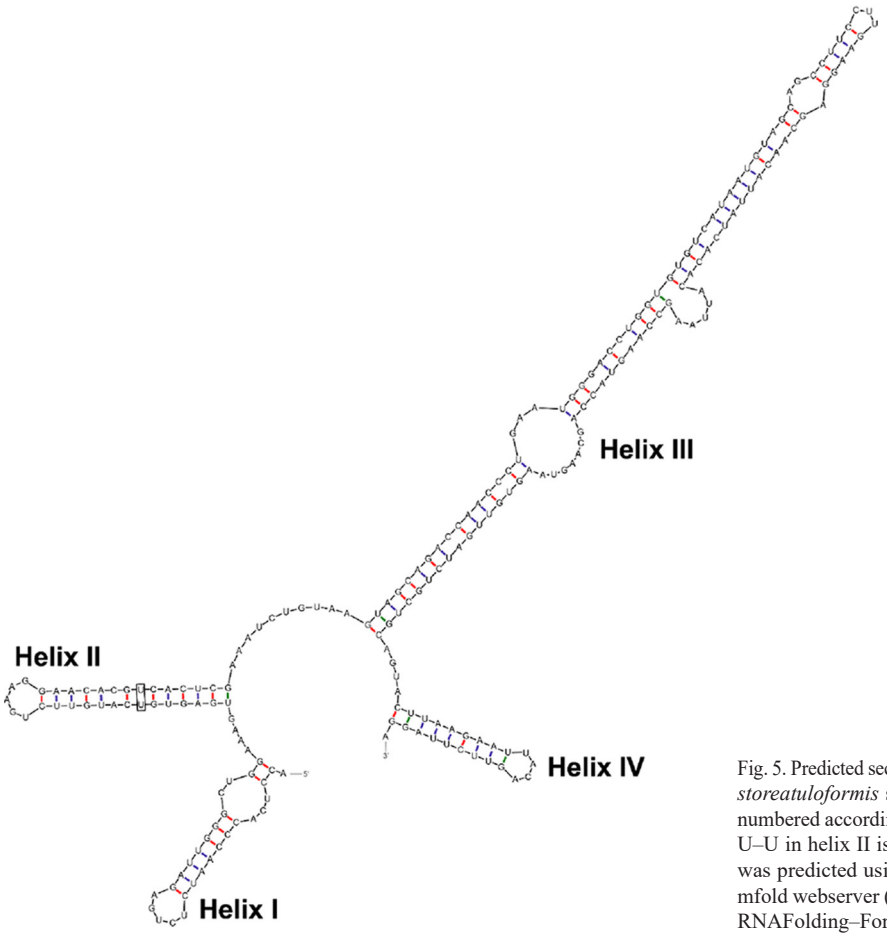

Fig. 5. Predicted secondary structure of ITS2 for *Rhodomonas storeatuloformis* sp. nov. (strain IBSS–59). Helices are numbered according to Coleman (2000). Typical unpaired U–U in helix II is marked by rectangular. The structure was predicted using RNA folding program available at mfold webserver (http://mfold.rna.albany.edu/?q=mfold/RNAFolding–Form).

(Fig. 6). A similar internal loop is described in the helix I in the three species (*R. storeatuloformis*, *Rhodomonas* sp. CCMP743 and *Rhodomonas* sp. CCMP763), while it is absent in *R. lens* CCMP739 and *Rhodomonas* sp. CCMP760 (Fig. 6). Across the strains, the helices I and II are quite variable in their terminal parts and in length.

Helix II in *R. storeatuloformis*, *Rhodomonas* sp. CCMP743, and *Rhodomonas* sp. CCMP763 has identical internal loop (Fig. 6) and a typical U–U mismatch that is highly conserved across different species (HOEF–EMDEN 2007). Helix II in *R. lens* CCMP739 has a bulge close to the U–U mismatch. Helix III in all compared strains is the longest, about twice the length of other helices (Fig. 6). All compared helices III have two internal terminal loops and one bulge, and *Rhodomonas* sp. CCMP763 has an additional loop. The helix III found in *R. storeatuloformis*, *Rhodomonas* spp. CCMP743 and CCMP763 is shorter than the helix III in *Rhodomonas* sp. CCMP760. Terminal part structures are highly conserved among strains. Helix IV in all compared strains has the similar structure, without any internal loops or bulges. Helix IV in *Rhodomonas* sp. CCMP760 is slightly longer than in other strains (Fig. 6).

CBCs between *R. storeatuloformis* and the closest strains were found in all four ITS2 helices (Table 2; Fig. 6). The largest number of CBCs between strains is revealed in helix III, and the lowest – in helix I. The number of CBCs between *R. storeatuloformis* and *Rhodomonas* sp. CCMP743 and *Rhodomonas* sp. CCMP763 is much lower than between *R. storeatuloformis* and *R. lens* CCMP739 and *Rhodomonas* sp. CCMP760 (Table 3). Therefore, *R. storeatuloformis* differs in no less than three CBCs from the other phylogenetically related strains.

DISCUSSION

In this study, a new cryptomonad species, *Rhodomonas storeatuloformis*, was established from the coastal waters of the northern Black Sea. The morphology of *R. storeatuloformis* is consistent with assignment of the species within the family Pyrenomonadaceae (NOVARINO & LUCAS 1993; CLAY et al. 1999) with respect to its typical ovoid cell shape and pyrenoid bridged two parts of H–shaped, bilobed and phycoerythrin–bearing chloroplast. The family Pyrenomonadaceae encompasses cryptomonads with distinctive pigment Cr–phycoerythrin 545 in plastids and nucleomorph imbedded within the pyrenoid (NOVARINO & LUCAS 1993; CLAY et al. 1999; CLAY 2015). Although the location of nucleomorph in relation to the pyrenoid in *R. storeatuloformis* was not shown in this study, its close relation to cryptomonad taxa with an intrapyrenoidal position of nucleomorph was confirmed by molecular data.

Fottea, Olomouc, 22(1): 122–136, 2022
DOI: 10.5507/fot.2021.019

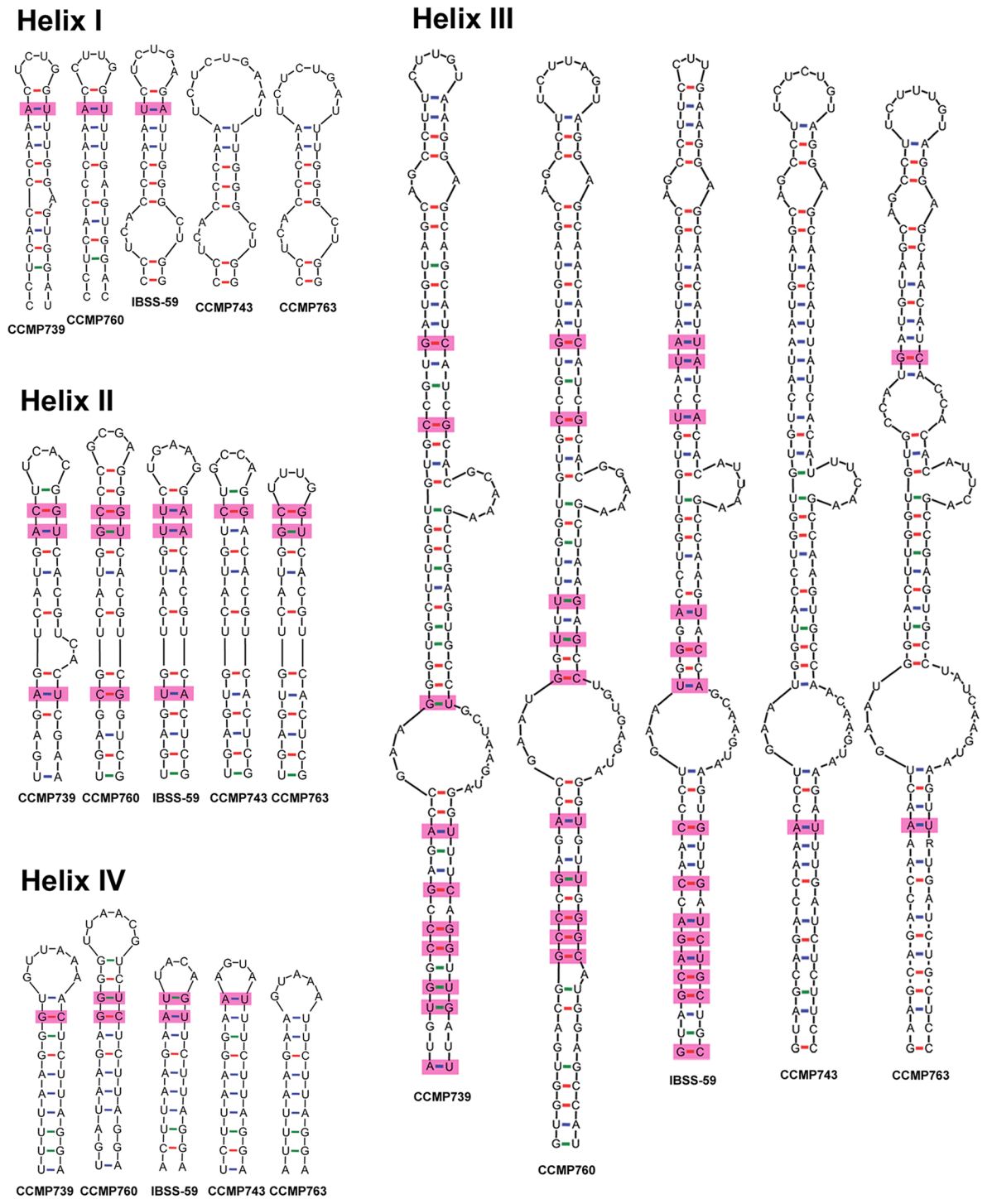

Fig. 6. Predicted secondary structures of ITS2 helices I, II, III and IV of *R. storeatuloformis* sp. nov. (IBSS–59) and four closest strains *Rhodomonas lens* CCMP739, *Rhodomonas* sp. CCMP760, *Rhodomonas* sp. CCMP743, and *Rhodomonas* sp. CCMP763. CBCs are marked by rectangular boxes and highlighted with pink background. The structure was predicted using RNA folding program available at mfold webserver (http://mfold.rna.albany.edu/?q=mfold/RNAFolding–Form).

Pyrenomonadaceae includes three genera namely *Rhodomonas* Karsten (syn. *Pyrenomonas* Santore), *Rhinomonas* Hill et Wetherbee, and *Storeatula* Hill (Clay et al. 1999; Clay 2015; Guiry & Guiry 2021). Hill & Wetherbee (1989) opened the still ongoing discussion regarding whether *Rhodomonas* Karsten emend. Hill et Wetherbee is synonymous with *Pyrenomonas*, or each genus should be considered separately (e.g. Hill & Wetherbee 1989; Novarino 2012). Currently, these generic names are conventional synonymous (Deane et al. 2002; Novarino 2003; Clay 2015; Guiry & Guiry 2021).

Recent molecular–based analyses confirmed the grouping of cryptomonad taxa with an intrapyrenoidal

Table 2. ITS and 5.8S sequence lengths (in bp) of *R. storeatuloformis* (strain IBSS–59) and closely related *Rhodomonas* strains.

Strain	ITS1	5.8S	ITS2
Rhodomonas storeatuloformis IBSS–59	311	155	225
Rhodomonas lens CCMP739	331	155	233
Rhodomonas sp. CCMP743	320	155	224
Rhodomonas sp. CCMP763	325	155	221
Rhodomonas sp. CCMP760	325	155	237

Table 3. Number of CBCs in ITS2 between *R. storeatuloformis* (strain IBSS–59) and closely related *Rhodomonas* strains.

Strain	Helix I	Helix II	Helix III	Helix IV	Total
Rhodomonas sp. CCMP743	–	1	1	1	3
Rhodomonas sp. CCMP763	–	2	2	–	4
Rhodomonas lens CCMP739	1	3	10	1	15
Rhodomonas sp. CCMP760	1	3	10	2	16

position of nucleomorph in robust monophyletic branch with three clades (Marin et al. 1998; Clay et al. 1999; Hoef–Emden et al. 2002; Deane et al. 2002; Lane et al. 2006; Shalchian–Tabrizi et al. 2008; Majaneva et al. 2014). To date, the number of described species in *Rhodomonas*/*Pyrenomonas* is about 40, and 10 species were identified in *Rhinomonas* (Novarino 2012), while the genus *Storeatula* includes only two described species from marine (Hill 1991) and freshwater (Kugrens et al. 1999) environments.

The genera within the family Pyrenomonadaceae were differentiated based on previously accepted as taxonomically significant LM and SEM–defined morphological characters including the type of inner periplast component (plated versus non–plated), the morphology of vestibular region of the cell from which the flagella arise (especially presence or absence of true, non–artefactual furrow), and presence/absence of mid–ventral band (Hill & Wetherbee 1988, 1989; Hill 1991; Kugrens et al. 1999; Novarino 2003, 2005, 2012; Majaneva et al. 2014; Table 4).

The appearance of *R. storeatuloformis* as observed by LM and SEM most closely matches the species of the genus *Storeatula* in terms of cell shape, plastidial and furrow/gullet complex, and periplast structure. In contrast to *R. storeatuloformis*, a highly lobed chloroplast and flagella of the equal length were described in the type species, marine *Storeatula major* (Table 4; Butcher 1967; Hill 1991; Cerino & Zingone 2006). However, these differences withdraw when compared with the freshwater *Storeatula rinosa*, which can only be distinguished from *R. storeatuloformis* by its habitat (Kugrens et al. 1999). *R. storeatuloformis* differs from *Rhodomonas baltica* (generitype) and other species of the genus *Rhodomonas* sensu Hill et Wetherbee (1989) by the absence of furrow and mid–ventral band. It is further distinguished from both *Rhodomonas* and *Rhinomonas* species by sheet-like inner periplast component without discrete plates versus rectangular inner periplast plates in *Rhodomonas* and hexagonal plates in *Rhinomonas* (Table 4; Hill & Wetherbee 1988, 1989; Cerino & Zingone 2006).

Among the other cryptomonad taxa originating from the Sevastopol Bay, *Cryptomonas flexa* differs from *R. storeatuloformis* in characteristic comma–shaped outline, smaller sizes, a longer gullet, and the presence of a furrow (Table 4; Rouchijajnen 1970). Two other *Cryptomonas* species, *C. rubra* and *C. vulgaris*, were described as having two chloroplasts compared to a single one in *R. storeatuloformis*. In both of these species, gullet is longer than in *R. storeatuloformis*, and *C. vulgaris* has a furrow, unlike in *R. storeatuloformis* (Table 4; Rouchijajnen 1967, 1971). A more complete morphological comparison of *R. storeatuloformis* with cryptomonad taxa from the same locality is limited due to the lack of SEM–based observation of cell morphology for previously described taxa and no type material available for re–examination since 1960–70s.

The morphological features of *R. storeatuloformis* (sheet–like inner periplast and the absence of a furrow and mid–ventral band) place it within the *Storeatula* (Hill 1991; Kugrens et al. 1999; Cerino & Zingone 2006) but separate it from both the representatives of the genus *Rhinomonas* with plated periplast and, especially,

Fottea, Olomouc, 22(1): 122–136, 2022
DOI: 10.5507/fot.2021.019

from the *Rhodomonas* species having plated periplast, a furrow and mid–ventral band (Hill & Wetherbee 1988, 1989). However, this morphologically–based assignment contradicts the results of our molecular analysis, which robustly grouped *R. storeatuloformis* with the *Rhodomonas* strains (Fig. 4).

Our analysis of predicted ITS2 secondary structures of the *R. storeatuloformis* (strain IBSS–59) and most closely related *Rhodomonas* strains revealed the compensatory base changes among the strains (Fig. 6). Following the concept that two organisms/strains whose ITS2 sequences differ by even a single CBC represent two different biological species (Coleman 2000; Müller et al. 2007; Wolf et al. 2013) we conclude that the strain IBSS–59 is a separate species. We named the new species as *Rhodomonas storeatuloformis* to point on its morphological similarity to the *Storeatula* species.

The taxonomic significance of the structural morphological differences used to distinguish the strains of the family Pyrenomonadaceae between *Rhinomonas, Storeatula,* and *Rhodomonas* genera have been rethought since the separation between genera was not supported by SSU rRNA phylogenies due to low sequence divergence (Marin et al. 1998). Recent studies have shown that the division of cryptophytes into species and genera based on their general morphology often contradicts with molecular phylogenies (Hoef–Emden 2007, 2012; Majaneva et al. 2014; Altenburger et al. 2020 and references therein), and the combined LM, SEM and molecular analyses are required to avoid taxonomic confusions and clarify the phylogeny.

Molecular phylogenetic studies revealed that although differences in biliprotein type correspond to the phylogeny, the type of inner periplast component is incompatible with the topology of molecular trees in many cryptomonad groups (Hoef–Emden et al. 2002; Hoef–Emden & Melkonian 2003). As a result, the monophyly of the genera with periplast–based delineation and their taxonomy were questioned (Hoef–Emden & Melkonian 2003; Lane et al. 2006; Shalchian–Tabrizi et al. 2008; Majaneva et al. 2014). In the family Pyrenomonadaceae, three different types of the inner periplast components were identified including periplast components with distinct either rectangular (*Rhodomonas*) or hexagonal (*Rhinomonas*) inner plates, and composed of a sheet–like layer in *Storeatula* (Hill & Wetherbee 1988, 1989; Hill 1991; Table 3). However, in the phylogenetic studies the strains with different periplast structures did not form separate clades, but were distributed throughout the phylogenetic trees (e.g. Deane et al. 2002; Hoef–Emden et al. 2002; Majaneva et al. 2014; this study). Previous molecular–based studies of the family Pyrenomonadaceae have shown monophyly of this cryptomonad group itself, whereas its largest genus *Rhodomonas* was found to be polyphyletic (Deane et al. 2002; Majaneva et al. 2014). Nuclear 18S rDNA phylogeny clustered the examined *Rhodomonas* strains either with *Rhinomonas* or with *Storeatula* (Deane et al. 2002).

Recent phylogenetic analyses based on a wide range of nuclear and nucleomorph ribosomal sequences have divided the strains belonging to the family Pyrenomonadaceae into three clades, one of which consisted of the *Rhinomonas* species, whereas the strains of *Rhodomonas* were distributed between two clades with some of them clustered with *Storeatula* strains (Majaneva et al. 2014). Our Bayesian tree based on the concatenated nuclear–encoded 18S and 28S rDNA genes and ITS region sequences (Fig. 4) has a topology similar to that of Majaneva et al. (2014). However, our results point on more complicated phylogenetic relationships across the strains of the family Pyrenomonadaceae. The crown clade on our Bayesian tree is analogous to the clade B (*Rhodomonas baltica* group in Majaneva et al. 2014), whereas two other clades (A and C, according to Majaneva et al. 2014) are not well supported by bootstrap on our Bayesian tree. Clade C splits into two branches: the first one consists of *Rhodomonas* and *Rhinomonas* supported by a moderate posterior probability 0.73 and the second one consist of two sequences of *Storeatula major* and uncultured cryptophyte Cr–MAL03. Clade A also splits into two branches: the first one consists of *Storeatula* and *Rhodomonas* strains with the high posterior probability of 1.0, and the second one consists of *Rhodomonas marina* and several unidentified *Rhodomonas* strains. Moreover, some *Rhodomonas* species form a separate clade, while others are grouped with *Storeatula* or *Rhinomonas* strains.

The integration of phylogenetic and morphological data questioned the current delineation of the genera within the family Pyrenomonadaceae. Our molecular phylogenetic analyses contradict with monophyly of both *Storeatula* and *Rhodomonas* genera and suggest that morphological characters used to distinguish species within the *Rhodomonas*/*Storeatula*/*Rhinomonas* group are unreliable. Despite the obvious morphological differences between the described *Rhodomonas* strains and the Black Sea strain IBSS–59, and its similarity to the *Storeatula* strains, our molecular analyses definitely placed the strain IBSS–59 within a well–supported clade of *Rhodomonas* strains but distantly from the *Storeatula* strains. The revealed contradiction between morphological and phylogenetic data may be explained by a potential heteromorphic life cycle or hidden dimorphism, which has already been hypothesized previously for some cryptomonads by Hoef–Emden et al. (2002), and for species of the family Pyrenomonadaceae in particular (Hoef–Emden et al. 2002; Majaneva et al. 2014). For instance, the haploid stage of *Proteomonas sulcata* possesses the periplast plates, while diploid stage is characterized by a sheet–like periplast structure (Hill & Wetherbee 1986; Cerino & Zingone 2006). At least five freshwater *Cryptomonas* strains have alternating morphotypes with periplast plates (called "cryptomorph") versus a sheet–like ("campylomorph") periplast (Hoef–Emden & Melkonian 2003). The *Storeatula* species possessing a sheet–like periplast were proposed as possible

Table 4. Comparison of morphological characteristics of *Rhodomonas storeatuloformis* sp. nov. with generitype species of the family Pyrenomonadaceae and with previously described cryptomonad species from Sevastopol Bay.

Species Character	***Rhodomonas storeatuloformis* sp.nov.**[a]	***Rhodomonas baltica* Karsten**[b]	***Rhinomonas pauca* Hill et Wetherbee**[c,d]	***Storeatula major* Hill**[d,e,f]	***Cryptomonas flexa* Roukhiyajneng**	***Cryptomonas rubra* Roukhiyajnenh**	***Cryptomonas vulgaris* Roukhiyajneni**
Cell shape, size, µm	ovoid, 12–19×5–10	oval, 12–40	broadly ovate to elliptic, 6–10×3.5–6 µm	ellipsoid, 12–20×5–10	Comma shaped, 8–12×**5**–6	ovoid 9–16×5–7	ovoid, 9–14.5×6–8.5
Plastids number, shape, color	1, bilobed, H–shaped, brown	1, bilobed, with ventral and posterior cuts, floridean red	1, bilobed, with narrow posterior extension, red–brown	1, highly lobed, brown	1, dorsal, green–brownish to brown–pinkish	2, brick–red	2, parietal, with crenulated margins, yellow–greenish
Pyrenoid	central, dorsal, with starch	central, dorsal, with starch	central, dorsal, with starch	central, dorsal, with starch	?	dorsal, posterior	Parietal, below midline, with starch
Flagella	unequal	unequal	unequal	equal	equal**	equal**	unequal**
Furrow*	–	+	–	–	+	+	?
Gullet	<1/3 cell length	1/2 cell length	c.a. 1/3 cell length	1/2 cell length	2/3 cell length	2/3 cell length	1/2 cell length
Vestibular ligule*	+	–	–	+	?	?	?
Mid–ventral band*	–	+	–	–	?	?	?
Periplast:							
inner component*	sheet without plates	rectangular plates	hexagonal plates	sheet without plates	?	?	?
superficial component	coarse fibrillar	fibrillar	fibrillar	coarse fibrillar	?	?	?

+, present; –, absent; ?, no data available; *, characters currently used to delineate genera in the family Pyrenomonadaceae; **, as seen from line–drawing; references: [a]this study; [b]HILL & WETHERBEE 1989; [c]HILL & WETHERBEE 1988; [d]CERINO & ZINGONE 2006; [e]BUTCHER 1967; [f]HILL 1991; [g]ROUCHIJAJNEN 1970; [h]ROUCHIJAJNEN 1967; [i]ROUCHIJAJNEN 1971.

Fottea, Olomouc, 22(1): 122–136, 2022
DOI: 10.5507/fot.2021.019

alternating morphotypes of *Rhodomonas* and *Rhinomonas* with periplast plates (Majaneva et al. 2014). Recently, one more example of dimorphism in cryptophytes was proposed representing different life stages of the same species with *Plagioselmis prolonga* (periplast with plates) as haploid stage and *Teleaulax amphioxeia* (sheet–like periplast) as diploid stage (Altenburger et al. 2020). However, to reveal the true dimorphism in the taxa, the further investigations of morphological features coupled with molecular analyses and ploidy study using clonal cultures of cryptophytes are required in order to make the classification of this group consistent with phylogeny.

Acknowledgments

The authors are grateful to Kerstin Hoef–Emden (University of Cologne, Cologne Biocenter, Botanical Institute, Germany), Federica Cerino (National Institute of Oceanography and Experimental Geophysics (OGS), Trieste, Italy) and Evgeniy S. Gusev (K.A. Timiryazev Institute of Plant Physiology RAS, Moscow, Russia) for their methodological consultancy. We thank Vyacheslav N. Lishaev (IBSS) for technical assistance with SEM. We wish to thank the Editor–in–Chief Prof. Aloisie Poulíčková and anonymous reviewer for their detailed and constructive comments. This work was financially supported by the Research Program of the Russian Academy of Sciences grant agreement # 121030300149–0 at the IBSS RAS (AK, OR, LA) and # AAAA–A17–117120540067–0 (VA, OP).

References

Adolf, J.E.; Place, A.R.; Stoecker, D.K. & Harding, L.W.Jr. (2007): Modulation of polyunsaturated fatty acids in mixotrophic *Karlodinium veneficum* (Dinophyceae) and its prey, *Storeatula major* (Cryptophyceae). – J. Phycol. 43: 1259–1270.

Altenburger, A.; Blossom, H.E.; Garcia–Cuetos, L.; Jakobsen, H.H.; Carstensen, J.; Lundholm, N.; Hansen, P.J.; Moestrup, Ø. & Haraguchi, L. (2020): Dimorphism in cryptophytes – The case of *Teleaulax amphioxeia*/*Plagioselmis prolonga* and its ecological implications. – Sci. Adv. 6: eabb1611.

Andersen, R.A. (2005): Algae Culturing Technique. – 578 pp., Elsevier Academic Press, New York.

Bermúdez, J.; Rosales, N.; Loreto, C.; Briceño, B. & Morales, E. (2004): Exopolysaccharide, pigment and protein production by the marine microalga *Chroomonas* sp. in semicontinuous cultures. – World J. Microbiol. Biotechnol. 20: 179–183.

Bistricki, T. & Munawar, M. (1978): A rapid preparation method for scanning electron microscopy of Lugol preserved algae. – J. Microsc. 114: 215–218.

Bourrain, M.; Achouak, W.; Urbain, V. & Heulin, T. (1999): DNA extraction from activated sludges. – Curr. Microbiol. 38: 315–319.

Buma, A.G.J.; Gieskes, W.W.C. & Thomsen, H.A. (1992): Abundance of Cryptophyceae and chlorophyll b–containing organisms in the Weddell–Scotia confluence area in the spring of 1988. – Polar. Biol. 12: 43–52.

Butcher, R.W. (1967): An Introductory Account of the Smaller Algae of British Coastal Waters. Part IV: Cryptophyceae. – Fishery Investigations, ser. IV, Ministry of Agriculture, Fisheries and Food, London.

Cerino, F. & Zingone, A. (2006): A survey of cryptomonad diversity and seasonality at a coastal Mediterranean site. – Eur. J. Phycol. 41: 363–378.

Cerino, F. & Zingone, A. (2007): Decrypting cryptomonads: A challenge for molecular taxonomy. – In: Brodie, J. & Lewis, J. (eds): Unravelling the Algae: the Past, Present, and Future of Algal Systematics, Vol. 75. – pp. 197–211, CRC Press, Boca Raton.

Clay, B.L. (2015): Cryptomonads. – In: Wehr, J., Sheath, R. & Kociolek, J.P. (eds): Freshwater Algae of North America. – pp. 809–850, Elsevier Inc, London, Waltham.

Clay, B.L.; Kugrens, P. & Lee R.E. (1999): A revised classification of Cryptophyta. – Bot. J. Linn. Soc. 131: 131–151.

Coleman, A.W. (2000): The significance of a coincidence between evolutionary landmarks found in mating affinity and a DNA sequence. – Protist 151: 1–9.

Coleman, A.W. (2007): Pan–eukaryote ITS2 homologies revealed by RNA secondary structure. – Nucleic Acids Res. 35: 3322–3329.

Coutinho, P.; Ferreira, M.; Freire, I. & Otero, A. (2020): Enriching rotifers with "premium" microalgae: *Rhodomonas lens*. – Mar. Biotechnol. 22: 118–129.

Czypionka, T.; Vargas, C.A.; Silva, N.; Daneri, G.; González, H.E. & Iriarte, J.L. (2011): Importance of mixotrophic nanoplankton in Aysen Fjord (Southern Chile) during austral winter. – Cont. Shelf Res. 31: 216–224.

Deane, J.A.; Strachan, I.M.; Saunders, G.W.; Hill, D.R. & McFadden, G.I. (2002): Cryptomonad evolution: nuclear 18S rDNA phylogeny versus cell morphology and pigmentation. – J. Phycol. 38: 1236–1244.

Dolgin, A. & Adolf, J. (2019): Scanning electron microscopy of phytoplankton: Achieving high quality images through the use of safer alternative chemical fixatives. – J. Young Investig. 37: 1–9.

Dunstan, G.A.; Brown, M.R. & Volkman, J.K. (2005): Cryptophyceae and Rhodophyceae; Chemotaxonomy, phylogeny, and application. – Phytochemistry 66: 2557–2570.

Edgar, R.C. (2004): MUSCLE: multiple sequence alignment with high accuracy and high throughput. – Nucleic Acids Res. 32: 1792–1797.

Fields, S.D. & Rhodes, R.G. (1991): Ingestion and retention of *Chroomonas* spp. (Cryptophyceae) by *Gymnodinium acidotum* (Dinophyceae). – J. Phycol. 27: 525–529.

Gelman, A. & Rubin, D.B. (1992): Inference from iterative simulation using multiple sequences. – Stat. Sci. 7: 457–472.

Gervais, F. (1997): Light-dependent growth, dark survival, and glucose uptake by cryptophytes isolated from a freshwater chemocline. – J. Phycol. 33: 18–25.

Guiry, M.D. & Guiry, G.M. (2021): AlgaeBase. – World–wide electronic publication, National University of Ireland, Galway. http://www.algaebase.org; searched on 24 February 2021.

Gusev, E.; Podunay, Y.; Martynenko, N.; Shkurina, N. & Kulikovskiy, M. (2020): Taxonomic studies of *Cryptomonas lundii* clade (Cryptophyta: Cryptophyceae) with description of a new species from Vietnam. – Fottea 20: 137–143.

Hall, T.A. (1999): BioEdit: A user–friendly biological sequence alignment editor and analysis program for Windows 95/98/NT. – Nucleic Acids Symp. Ser. 41: 95–98.

Hammer, A.C. & Pitchford, J.W. (2006): Mixotrophy, allelopathy and the population dynamics of phagotrophic algae (cryptophytes) in the Darss Zingst Bodden estuary, southern Baltic. – Mar. Ecol. Prog. Ser. 328: 105–115.

Han, M.S. & Furuya, K. (2000): Size and species–specific

primary productivity and community structure of phytoplankton in Tokyo Bay. – J. Plankton Res. 22: 1221–1235.

Hill, D.R.A. (1991): A revised circumscription of *Cryptomonas* (Cryptopbyceae) based on examination of Australian strains. – Phycologia 30: 170–188.

Hill, D.R. & Wetherbee, R. (1986): *Proteomonas sulcata* gen. et sp. nov. (Cryptophyceae), a cryptomonad with two morphologically distinct and alternating forms. – Phycologia 25: 521–543.

Hill, D.R.A. & Wetherbee, R. (1988): The structure and taxonomy of *Rhinomonas pauca* gen. et sp. nov. (Cryptophyceae). – Phycologia 27: 355–365.

Hill, D.R.A. & Wetherbee, R. (1989): A reappraisal of the genus *Rhodomonas* (Cryptophyceae). – Phycologia 28: 143–158.

Hoef–Emden, K. (2007): Revision of the genus *Cryptomonas* (Cryptophyceae) II: Incongruences between the classical morphospecies concept and molecular phylogeny in smaller pyrenoid–less cells. – Phycologia 46: 402–428.

Hoef-Emden, K. (2008): Molecular phylogeny of phycocyanin-containing cryptophytes: evolution of biliproteins and geographical distribution. – J. Phycol. 44: 985–993.

Hoef–Emden, K. (2012): Pitfalls of establishing DNA barcoding systems in protists: the cryptophyceae as a test case. – PLoS One 7: e43652.

Hoef–Emden, K. & Melkonian, M. (2003): Revision of the genus *Cryptomonas* (Cryptophyceae): a combination of molecular phylogeny and morphology provides insights into a long–hidden dimorphism. – Protist 154: 371–409.

Hoef–Emden K. & Archibald J.M. (2016): Cryptophyta (Cryptomonads). – In: Archibald, J.M. Simpson, A.G.B. & Slamovits, C.H. (eds): Handbook of the Protists. – pp. 851–891, Springer International Publishing, Cham, Switzerland.

Hoef–Emden, K.; Marin, B. & Melkonian, M. (2002): Nuclear and nucleomorph SSU rDNA phylogeny in the Cryptophyta and the evolution of cryptophyte diversity. – J. Mol. Evol. 55: 161–179.

Johnson, M.D.; Beaudoin D.J.; Laza–Martinez, A.; Dyhrman, S.T.; Fensin, E.; Lin, S. & Stoecker, D.K. (2016): The genetic diversity of *Mesodinium* and associated cryptophytes. – Front. Microbiol. 7: 2017.

Khanaychenko, A.N. (1999): The effect of microalgal diet on copepod reproduction parameters. – Ekologia Morya 49: 56–61 (in Russian, with summary in English).

Khanaychenko, A.; Mukhanov, V.; Aganesova, L.; Besiktepe, S. & Gavrilova, N. (2018): Grazing and feeding selectivity of *Oithona davisae* in the Black Sea: Importance of cryptophytes. – Turkish J. Fish. Aquat. Sci. 18: 937–949.

Kim, H.S.; Kim, J.H.; Jo, S.G.; Rho, J.R. & Yih, W. (2020): Amino acids and fatty acids composition in mass-cultured *Teleaulax amphioxeia* strains with notable potential for rotifer (*Brachionus plicatilis*) enrichment. – J. World Aquac. Soc. 51: 712–728.

Klaveness, D. (1988): Ecology of the Cryptomonadida: A first review. – In: Growth and Reproductive Strategies of Freshwater Phytoplankton. – pp. 105–33, Cambridge University Press, Cambridge.

Krasnova, E.D.; Pantyulin, A.N.; Matorin, D.N.; Todorenko, D.A.; Belevich, T.A.; Milyutina, I.A. & Voronov, D.A. (2014): Cryptomonad alga *Rhodomonas* sp. (Cryptophyta, Pyrenomonadaceae) bloom in the redox zone of the basins separating from the White Sea. – Microbiology 83: 270–277.

Kugrens, P.; Clay, B.L. & Lee, R.E. (1999): Ultrastructure and systematics of two new freshwater red cryptomonads, *Storeatula rhinosa*, sp. nov. and *Pyrenomonas ovalis*, sp. nov. – J. Phycol. 35: 1079–1089.

Lane, C.E.; Khan, H.; MacKinnon, M.; Fong, A.; Theophilou, S. & Archibald, J.M. (2006): Insight into the diversity and evolution of the cryptomonad nucleomorph genome. – Mol. Biol. Evol. 23: 856–865.

Laza-Martínez, A. (2012): *Urgorri complanatus* gen. et sp. nov. (Cryptophyceae), a red-tide-forming species in brackish waters. – J. Phycol. 48: 423–435.

Majaneva, M.; Remonen, I.; Rintala, J.–M.; Belevich, I.; Kremp, A.; Setälä, O. & Blomster, J. (2014): *Rhinomonas nottbecki* n. sp. (Cryptomonadales) and molecular phylogeny of the family Pyrenomonadaceae. – J. Eukaryot. Microbiol. 61: 480–492.

Marin, B.; Klingberg, M. & Melkonian, M. (1998): Phylogenetic relationships among the Cryptophyta: analyses of nuclear–encoded SSU rRNA sequences support the monophyly of extant plastid–containing lineages. – Protist 149: 265–276.

Marshall, W. & Laybourn–Parry, J. (2002): The balance between photosynthesis and grazing in Antarctic mixotrophic cryptophytes during summer. – Freshwater Biol. 47: 2060–2070.

Medlin, L.K. & Schmidt, K. (2010): Molecular probes improve the taxonomic resolution of Cryptophyte abundance in Arcachon Bay, France. – Vie et Milieu 60: 9–15.

Medlin, L.K.; Piwosz, K. & Metfies, K. (2017): Uncovering hidden biodiversity in the Cryptophyta: Clone library studies at the Helgoland time series site in the Southern German Bight indentifies the cryptophycean clade potentially responsible for the majority of its genetic diversity during the spring bloom. – Vie et Milieu 67: 27–32.

Milyutina, I.A.; Aleshin, V.V.; Mikrjukov, K.A.; Kedrova, O.S. & Petrov, N.B. (2001): The unusually long small subunit ribosomal RNA gene found in amitochondriate amoeboflagellate *Pelomyxa palustris*: its rRNA predicted secondary structure and phylogenetic implication. – Gene 272: 131–139.

Moncheva, S.; Boicenco, L.; Mikaelyan, A.S.; Zotov, A.; Dereziuk, N.; Gvarishvili, C.; Slabakova, N.; Mavrodieva, R.; Vlas, O.; Pautova, L.A.; Silkin, V.A.; Medinets, V.; Sahin, F. & Feyzioglu, A.M. (2019): Phytoplankton. – In: Black Sea State of Environment Report 2009–2014/5. – pp. 225–284, Commission on the Protection of the Black Sea Against Pollution, Istanbul.

Müller, T.; Philippi, N.; Dandekar, T.; Schultz, J. & Wolf, M. (2007): Distinguishing species. – RNA 13: 1469–1472.

Nakamura, Y. & Hirata, A. (2006): Plankton community structure and trophic interactions in a shallow and eutrophic estuarine system, Ariake Sound, Japan. – Aquat. Microb. Ecol. 44: 45–57.

Nesterova, D.A., Terenko, L.M. & Terenko, G.V. (2006): Phytoplankton species list. – In: Zaytsev, Yu.P. & Alexandrov, B.G. (eds.): Northwestern Part of the Black Sea: Biology and Ecology. – pp. 557–576, Naukova Dumka, Kiev.

Nguyen, L.T.; Schmidt, H.A.; Von Haeseler, A. & Minh, B.Q. (2015): IQ–TREE: A fast and effective stochastic algorithm for estimating maximum–likelihood phylogenies. – Mol. Biol. Evol. 32: 268–274.

Fottea, Olomouc, 22(1): 122–136, 2022
DOI: 10.5507/fot.2021.019

Novarino, G. (2003): A companion to the identification of cryptomonad flagellates (Cryptophyceae = Cryptomonadea). – Hydrobiologia 502: 225–270.

Novarino, G. (2005): Nanoplankton protists from the western Mediterranean Sea. II. Cryptomonads (Cryptophyceae = Cryptomonadea). – Sci. Mar. 69: 47–74.

Novarino, G. (2012): Cryptomonad taxonomy in the 21st century: The first two hundred years. – In: Wolowski, K., Kaczmarska, I., Ehrman, J. M. & Wojtal, A. (eds): Phycological Reports: Current Advances in Algal Taxonomy and its Applications: Phylogenetic, Ecological and Applied Perspective. – pp. 19–52, Institute of Botany, Polish Academy of Sciences, Krakow.

Novarino, G. & Lucas, I.A.N. (1993): Some proposals for a new classification system of the Cryptophyceae. – Bot. J. Linn. Soc. 111: 3–21.

Peltomaa, E.; Johnson, M.D. & Taipale, S.J. (2018): Marine cryptophytes are great sources of EPA and DHA. – Mar. Drugs 16: 1–11.

Polikarpov, I.; Saburova, M. & Al–Yamani, F. (2020): Decadal changes in diversity and occurrence of microalgal blooms in the NW Arabian/Persian Gulf. – Deep Sea Res. Pt II 179: 104810.

Roberts, E.C. & Laybourn–Parry, J. (1999): Mixotrophic cryptophytes and their predators in the Dry Valley lakes of Antarctica. – Freshwater Biol. 41: 737–746.

Ronquist, F.; Teslenko, M.; Van Der Mark, P.; Ayres, D.L.; Darling, A.; Höhna, S.; Larget, B.; Liu, L.; Suchard, M.A. & Huelsenbeck, J.P. (2012): MrBayes 3.2: Efficient Bayesian phylogenetic inference and model choice across a large model space. – Syst. Biol. 61: 539–542.

Rouchijajnen, M.I. (1967): Species nova generis *Cryptomonas* (Pyrrophyta) e mari Nigro (Ponto Euxino). – Novitates systematicae plantarum non vascularium / Novosti sistematiki nizshikh rastenii 4: 71–73 (in Russian, with Latin diagnosis).

Rouchijajnen, M.I. (1970): Species novae generum *Cryptomonas* (Pyrrophyta) et *Platymonas* (Chlorophyta, Chlamydomonadales) e mari Nigro. – Novitates systematicae plantarum non vascularium / Novosti sistematiki nizshikh rastenii 7: 20–23 (in Russian, with Latin diagnosis).

Rouchijajnen, M.I. (1971): De flagellatis nonnullis Maris Nigris notula. – Novitates systematicae plantarum non vascularium / Novosti sistematiki nizshikh rastenii 8: 3–9 (in Russian, with Latin diagnosis).

Seixas, P.; Coutinho, P.; Ferreira, M. & Otero, A. (2009): Nutritional value of the cryptophyte *Rhodomonas lens* for *Artemia* sp. – J. Exp. Mar. Biol. Ecol. 381: 1–9.

Senicheva, M.I. (2008): Species diversity, seasonal and interannual variability microalgae in plankton off the coast of Crimea. – In: Tokarev, Yu.N., Finenko, Z.Z. & Shadrin, N.V. (eds.): The Black Sea Microalgae: Problems of Biodiversity Preservation and Biotechnological usage. – pp. 5–17, NAS of Ukraine, Institute of Biology of the Southern Seas, ECOSI Gidrofizika, Sevastopol (in Russian).

Shalchian-Tabrizi, K.; Bråte, J.; Logares, R.; Klaveness, D.; Berney, C. & Jakobsen, K.S. (2008): Diversification of unicellular eukaryotes: cryptomonad colonizations of marine and fresh waters inferred from revised 18S rRNA phylogeny. – Environ. Microbiol. 10: 2635–2644.

Støttrup, J.G.; Richardson, K.; Kirkegaard, E. & Pihl, N.J. (1986): The cultivation of *Acartia tonsa* Dana for use as a live food source for marine fish larvae. – Aquaculture 52: 87–96.

Šupraha, L.; Bosak, S.; Ljubešić, Z.; Mihanović, H.; Olujić, G.; Mikac, I. & Viličić, D. (2014): Cryptophyte bloom in a Mediterranean estuary: High abundance of *Plagioselmis* cf. *prolonga* in the Krka River estuary (eastern Adriatic Sea). – Sci. Mar. 78: 329–338.

Tamura, K.; Stecher, G.; Peterson, D.; Filipski, A. & Kumar, S. (2013): MEGA6: Molecular evolutionary genetics analysis version 6.0. – Mol. Biol. Evol. 30: 2725–2729.

Van der Auwera, G.; Chapelle, S. & De Wachter, R. (1994): Structure of the large ribosomal subunit RNA of *Phytophtora megasperma*, and phylogeny of the oomycetes. – FEBS Lett. 338: 133–136.

Wolf, M.; Chen, S.; Song, J.; Ankenbrand, M. & Müller, T. (2013): Compensatory base changes in ITS2 secondary structures correlate with the biological species concept despite intragenomic variability in ITS2 sequences – a proof of concept. – PLoS One 8(6): e66726.

Yoo, Y.D.; Seong, K.A.; Jeong, H.J.; Yih, W.; Rho, J.R.; Nam, S.W. & Kim, H.S. (2017): Mixotrophy in the marine red–tide cryptophyte *Teleaulax amphioxeia* and ingestion and grazing impact of cryptophytes on natural populations of bacteria in Korean coastal waters. – Harmful Algae 68: 105–117.

Zhang, J.; Wu, C.; Pellegrini, D.; Romano, G.; Esposito, F.; Ianora, A. & Buttino, I. (2013): Effects of different monoalgal diets on egg production, hatching success and apoptosis induction in a Mediterranean population of the calanoid copepod *Acartia tonsa* (Dana). – Aquaculture 400: 65–72.

Zuker, M. (2003): Mfold web server for nucleic acid folding and hybridization prediction. – Nucleic Acids Res. 31: 3406–3415.

Supplementary material

The following supplementary material is available for this article:

Fig. S1. Culture of the strain IBSS–59 in flasks at different phases of exponential growth (increasing cell concentration from right to left) with increasing the intensity of the typical light brown color of culture.

This material is available as part of the online article (http://fottea.czechphycology.cz/contents)

Received May 25, 2021
Accepted September 29, 2021